Spatial mapping of ices in the Oph-F core

A direct measurement of CO depletion and the formation of CO_2

K. M. Pontoppidan[1,2]

[1] California Institute of Technology, Division for Geological and Planetary Sciences, MS 150-21, Pasadena, CA 91125, USA
e-mail: pontoppi@gps.caltech.edu
[2] Leiden Observatory, P.O. Box 9513, NL-2300 RA, Leiden, The Netherlands

ABSTRACT

Aims. Ices in dense star-forming cores contain the bulk of volatile molecules apart from H_2 and thus represent a large fraction of dark cloud chemistry budget. Mm observations of gas provide indirect evidence for significant freeze-out of CO in the densest cores. To directly constrain the freeze-out profile of CO, the formation route of CO_2 and the carrier of the $6.8\,\mu m$ band, the spatial distribution of the CO/CO_2 ice system and the $6.8\,\mu m$ band carrier are measured in a nearby dense core.
Methods. VLT-ISAAC, ISOCAM-CVF and Spitzer-IRS archival mid-infrared (3-$20\,\mu m$) spectroscopy of young stellar objects is used to construct a map of the abundances of CO and CO_2 ices in the Oph-F star-forming core, probing core radii from 2×10^3 to 14×10^3 AU or densities from 5×10^4 to 5×10^5 cm^{-3} with a resolution of ~ 3000 AU.
Results. The line-of-sight averaged abundances relative to water ice of both CO and CO_2 ices increase monotonously with decreasing distance to the core center. The map traces the shape of the CO abundance profile between freeze-out ratios of 5–60% and shows that the CO_2 ice abundance increases by a factor of 2 as the CO freezes out. It is suggested that this indicates a formation route of CO_2 on a CO ice surface to produce a CO_2 component dilute in CO ice, in addition to a fraction of the CO_2 formed at lower densities along with the water ice mantle. It is predicted that the CO_2 bending mode band profile should reflect a high $CO:CO_2$ number ratio in the densest parts of dark clouds. In contrast to CO and CO_2, the abundance of the carrier of the $6.8\,\mu m$ band remains relatively constant throughout the core. A simple freeze-out model of the CO abundance profile is used to estimate the binding energy of CO on a CO ice surface to 814 ± 30 K.

Key words. Astrochemistry – Molecular processes – ISM:Molecules – Infrared: ISM

1. Introduction

Theory has long predicted that molecules freeze out onto dust grains in dense molecular clouds causing gas-phase abundances to drop by orders of magnitude. A series of recent measurements of the gas-phase abundances of volatile molecules such as CO and N_2H^+ in dense cores have corroborated this conjecture (e.g. Caselli et al. 1999; Bacmann et al. 2002; Tafalla et al. 2004). CO ice has also been observed directly along a growing sample of isolated lines of sight toward both embedded young stellar objects as well as background stars, showing that the CO molecules taken from the gas-phase reappears in the solid phase (Chiar et al. 1994; Pontoppidan et al. 2003). CO ice is an excellent tracer of freeze-out processes because it is the only abundant ice species known to form initially in the gas-phase before adsorbing to a grain surface.

Pontoppidan et al. (2004) introduced the technique of ice mapping at high (~ 1000 AU) spatial resolution – comparable to that of gas-phase maps. The procedure was demonstrated by constructing a map of the distribution of water and methanol ices in the outer envelope of the class 0 protostar SMM 4 in the Serpens star-forming cloud. The ice map of SMM 4 was used to show that the water ice abundace remained constant over a relatively wide range of densities, while the methanol abundance increased sharply by at least a factor of ten within $10\,000$ AU of the center of SMM 4. In principle, ices are best mapped toward field stars located behind the cloud. However, such background stars are typically extremely faint in the mid-infrared wavelength region. Therefore, disk sources embedded in their parent molecular cloud core offer a convenient infrared continuum against which the ices in the core can be mapped, with appropriate caveats on the interpretation of the derived ice abundances.

Direct mapping of CO ice abundances is highly complementary to mapping of gas phase abundances, because ice maps are sensitive to depletion fractions as low as 5%, while gas-phase abundance maps trace high depletion factors (n(ice)/n(gas)) of $\gtrsim$ 50% (Caselli et al. 1999). Furthermore, the depletion fraction as a function of gas density in a core is strongly dependent on the properties of the dust grain surfaces. Direct maps of CO ice in a dense core therefore enables an independent measure of surface binding energies.

This letter presents the first spatial map of CO and CO_2 ices in a dense molecular core. *It will be demonstrated that by directly measuring the relation between ice abundances and gas densities, the following quantities can be constrained: 1) the dependence of CO depletion on gas density with a large dynamical range, 2) the CO-CO binding energy, 3) the formation route of CO_2 and the 6.8 μm band carrier.* The case study is the F core in the Ophiuchus molecular cloud complex (Motte et al. (1998)). Embedded within this region, are at least 8–10 infrared-bright young stars. The lines of sight toward 5 of these young stars are used to probe the ices in front of each star in order to obtain a cross section of ice abundances across the minor axis of the core.

2. Observations

The individual spectra are taken from van Dishoeck et al. (2003) and Pontoppidan et al. (2003) of the 3.08 μm and 4.67 μm stretching modes of solid H_2O and CO, obtained with the Infrared Spectrometer And Array Camera (ISAAC) on the Very Large Telescope (VLT) [1]. The solid CO_2 component is probed along the same lines of sight using the InfraRed Spectrograph (IRS) on the Spitzer Space Telescope (AOR IDs 0009346048 and 0009829888 [2]) (Pontoppidan et al. 2005; Lahuis et al. 2006) as well as 5-16.3 μm spectra obtained with ISOCAM-CVF (TDTs 29601715 and 29601813) (Alexander et al. 2003) [3]. The Spitzer spectra were taken as part of the Cores to Disks Legacy program (Evans et al. 2003). Combining these facilities, high quality 3-16 μm spectra are available for 5 sources within a radius of 15 000 AU from the center of the pre-stellar core, defined to be the 850 μm peak of Oph-F MM2 (α=16^{h}27 24.3, δ=-24°40 35, J2000) (Motte et al. 1998). Only IRS 46 has no suitable spectrum between 5 and 10 μm.

To determine the optical depths of the various ice bands continua were fitted using low-order polynomia. The CO and CO_2 bands are sufficiently narrow to make the continuum determination relatively straight-forward and unbiased. For the 3.08 μm water ice band a continuum is fitted to points between
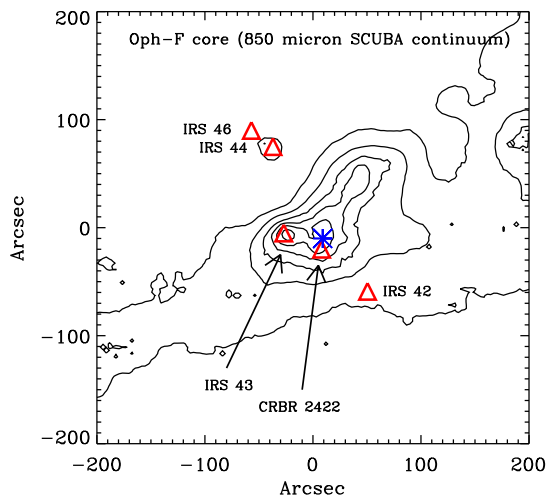

Fig. 2. The locations (triangles) of the sources used to construct the ice map plotted on the SCUBA 850 μm map. The star symbol indicates the center of the core.

3.8 to 4.0 μm and a K-band photometric point from the 2MASS catalogue. Finally, a local continuum between 5.5 and 8.0 μm is used to extract optical depth spectra of the 6.8 μm band. In consideration of the uncertainties in the continuum determination, care was taken to use the same "ice-free" regions and 2-order polynomia for all sources. Further discussion of the determination of continua for extracting ice optical depth spectra can be found in e.g. Gerakines et al. (1995); Dartois et al. (2002); Keane et al. (2001). The ice spectra are shown on an optical depth scale in Fig. 1, while the locations of the sources relative to an 850 μm JCMT-SCUBA map obtained by the COMPLETE collaboration (Ridge et al. 2006) are shown in Fig. 2.

The CO ice column densities have been determined in Pontoppidan et al. (2003). For the water 3.08 μm band and the CO_2 15.2 μm band, band strengths of 2.0×10^{-16} cm molecule^{-1} and 1.1×10^{-17} cm molecule^{-1} are used, respectively (Gerakines et al. 1995). For the 6.8 μm band, a band strength of 4.4×10^{-17} cm/ molecule^{-1} is assumed, appropriate for NH_4^+ (Schutte & Khanna 2003). The ice column densities are summarized in Table 1.

3. Abundance profiles of CO and CO_2 ice

The basic ice map is constructed by determining the ice column densities along each line of sight and ratioing with the water ice column density. The implicit assumption is that the 3.08 μm water ice band traces the total H_2 column density (see Pontoppidan et al. (2004) for a discussion). This yields CO and CO_2 line-of-sight averaged ice abundances relative to H_2O ice as a function of projected distance to the center of the core. The radial map is shown in Fig. 3.

It is seen that the abundances of pure CO, water-rich CO and CO_2 all increase toward the center of the core, while the 6.8 μm band carrier decreases slightly in abundance. The sharp rise in CO ice abundance is expected for CO freezing out from the gas-phase at high densities in the central parts of the core.
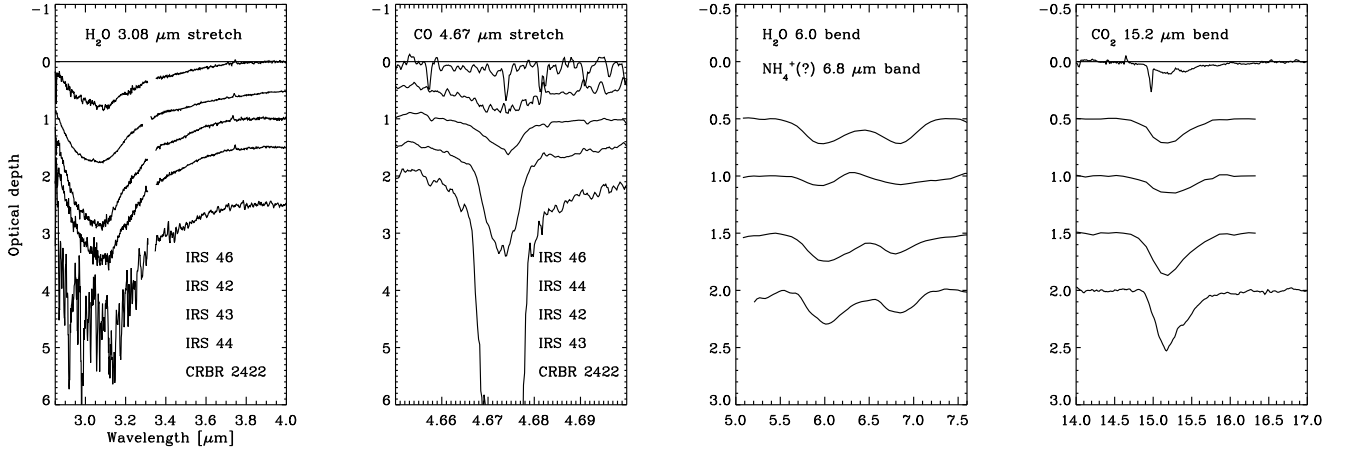
Fig. 1. Overview of the H_2O, CO, $6.8\,\mu m$ and CO_2 ice bands (ordered left to right) used to construct the ice map of the Oph-F core. The $3.08\,\mu m$ water ice bands shown on the left-most panel are ordered according to optical depth, for clarity, as indicated in the panel. In the remaining panels, the sources are ordered according to projected distance to the core center, with the source furthest from the center (IRS 46) at the top. No $5-8\,\mu m$ spectrum is available for IRS 46. Note also that the $6.8\,\mu m$ band of IRS 42 is filled in by emission likely due to PAHs. All the spectra have been shifted vertically, for clarity.

Table 1. Line-of-sight averaged ice abundances in the Oph-F core

	CBRR 2422.8-3423	IRS 43	IRS 42	IRS 44	IRS 46
Distance to Oph-F MM2 [AU]	1.8e3	4.3e3	8.2e3	11.0e3	13.9e3
$N(H_2O)$ [cm^{-2}]	3.9e18	2.96e18	1.87e18	3.04e18	1.17e18
$N(Pure\ CO)/N(H_2O)$	0.78	0.32	0.15	0.06	0.05
$N(CO\ in\ water)/N(H_2O)$	0.19	0.073	0.05	0.04	0.0
$N(CO_2)/N(H_2O)$	0.32	0.24	0.184	0.154	0.103
$N(6.8)/N(H_2O)$[1]	0.08	0.10	–	0.12	–
	ISAAC/IRS	ISAAC/ISOCAM	ISAAC/ISOCAM	ISAAC/ISOCAM	ISAAC/IRS

Assuming a constant water ice abundance of 9×10^{-5} relative to H_2 in accordance with a model of the CRBR 2422.8-3423 line of sight of Pontoppidan et al. (2005), the average abundance of pure CO ice is seen to rise from 4.5×10^{-6} to 7.0×10^{-5}, and the total CO and CO_2 abundances from 2.3×10^{-5} to 12×10^{-5}. This corresponds to a total CO depletion ranging from 12% to 60%, assuming an initial CO gas-phase abundance of 2×10^{-4}.

The increase by roughly a factor two in CO_2 ice abundance is particularly interesting. Since CO_2 molecules are formed on the grain surfaces, the increase in CO_2 ice abundance along with the CO freeze out is a direct indication of a formation route associated with CO. A significant amount of CO_2 is present in the outer parts of the Oph-F core where the densities are not yet high enough for the CO to freeze out. *This can be interpreted as evidence for two distinct eras for CO_2 ice formation*: The first takes place at roughly the same time as the bulk of the water ice is formed, which is known to happen as soon as the extinction, A_V, into the cloud reaches a specific, relatively low, threshold of roughly 3-5 magnitudes (Whittet et al. 1988). This domain is not probed by the Oph-F ice map. The second takes place during the catastrophic freeze-out of CO that occurs at densities of a few 10^5 cm^{-3} (Jørgensen et al. 2005) in which an almost pure CO ice mantle forms. This second phase of CO_2 molecules should be easily detectable in the shape of the

$15.2\,\mu m$ CO_2 bending mode absorption band, which is highly sensitive to the molecular environment of the CO_2 molecules. Specifically, the new CO_2 molecules should be found to be dilute in the CO ice with an average fraction of 1:5, as determined by the relative CO and CO_2 abundance increases in the Oph-F core. Since the CO freeze-out rate is a very strongly increasing function of density, it is expected that the CO_2:CO ratio will decrease in denser parts of the core. Thus, one would expect to find a range of components in the CO_2 bending mode in the centers of dense clouds. The spectral resolution of the ISOCAM-CVF spectra ($\lambda/\Delta\lambda \sim 50$) is not sufficiently high to search for such band shape changes in the current data.

Since the young stars that are used to estimate ice abundances in the core material are embedded in the core, significant caveats apply. Heating of the core material may desorb CO ice within a radius of a few hundred AU of each source, depending on the luminosity. However, since the projected size of the core is 30 000 AU, desorption is likely to play only a minor role. A possible exception to this is IRS 46, which contains a significant component of warm molecular gas along the line of sight (Lahuis et al. 2006). Also, the sources may be surrounded by remnant envelopes with different ice abundances than the surrounding core. The ice absorption toward CRBR 2422.8-3423 was shown by Pontoppidan et al. (2005) to be dominated
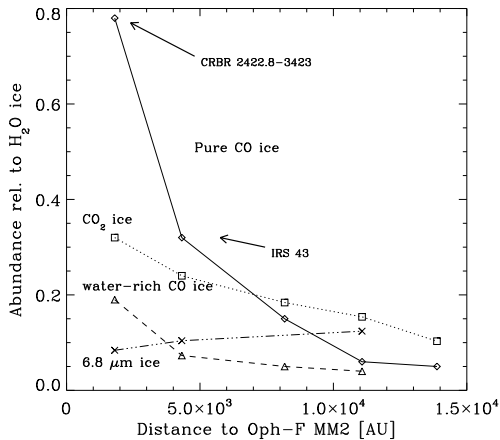
Fig. 3. Radial map of CO and CO_2 ices of the Oph-F core. Ice abundances relative to H_2O ice toward young stars are plotted as functions of projected distance to the center of the core as described in the text. The CO ice has been split into a "pure" and "water-rich" component following Pontoppidan et al. (2003).

by cold core material, although a fraction of the water, CO_2 and $6.8\,\mu m$ ices are likely located in the disk. However, it was found that the CO ice observed in this line of sight could not originate in the disk.

4. Empirical determination of the CO-CO binding energy

The CO depletion profile in Fig. 3 is modeled using a simplified freeze-out model, assuming a static core and that only thermal desorption occurs. For the purposes of this letter, the model presented is intended as a demonstration of the method, rather than achieving very accurate results. The rate of ice mantle build-up is then given by:

$$\frac{dn_{ice}}{dt} = R_{ads} - R_{des}, \tag{1}$$

Where $R_{des} = \nu_0 \exp[-dH/kT] \times n_{CO,ice} \times \beta$ is the desorption rate and $R_{ads} = n_{CO,gas} \times n_{dust} \times \pi d^2 \times \sqrt{3kT/m_{CO}} \times f$ is the adsorption rate. β is a factor taking into account that CO only desorbs from the top monolayer (i.e. 1st order desorption for sub-monolayer coverage and 0th order desorption for multilayers). $d = 0.05\,\mu m$ is the grain radius, $f = 1$ is the sticking coefficient, ν_0 is the frequency of the CO stretching mode and $n_{CO,gas}$ and n_{dust} are the number densities of CO gas and dust particles. Solving for n_{ice} yields a time dependent ice density given a gas density and (assumed identical) gas and dust temperature. This rate equation reaches an equilibrium on relatively short time scales ($<< 10^6$ years). Therefore, given a temperature and density structure, one can in principle solve for the binding energy of CO, dH. For the density profile of the core, a Bonnor-Ebert sphere with a central density of 5.5×10^5 cm^{-3} is used with a temperature of 15 K as suggested by Motte et al. (1998) and references therein. This simple procedure yields a CO on CO binding energy of 814 ± 30 K. The
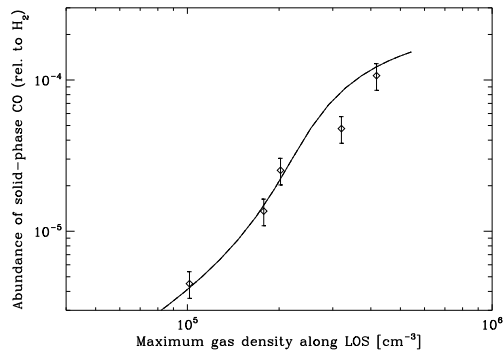

Fig. 4. Observed and modeled CO ice abundance for Oph-F. The curve shows the simple freeze-out model for the best-fitting CO binding energy of $dH/k = 814$ K. The "solid CO" abundance is the sum of the pure CO, CO in water and the CO_2 ice excess abundances. This assumes that one CO molecule is used to produce each CO_2 molecule. The error bars indicate a 20% uncertainty.

uncertainty reflects different results obtained if varying the central density and water ice abundance by 50%. Additionally, the derived binding energy scales linearly with the assumed dust temperature. Considering the simplified analysis, this result is consistent with that recently found by Bisschop et al. (2006) from laboratory experiments.

The radial map constitutes the first direct observation of the freeze-out profile of CO on dust grains in a prestellar core previously inferred indirectly from observations of millimetre lines of molecules. Additionally the observed increase in CO_2 ice abundance toward the center is the first quantitative observational evidence of the formation of CO_2 from CO on the surfaces of dust grains. These are observations that would not have been possible with single lines of sight.

References

Alexander, R. D., Casali, M. M., André, P., Persi, P., & Eiroa, C. 2003, A&A, 401, 613

Bacmann, A., Lefloch, B., Ceccarelli, C., et al. 2002, A&A, 389, L6

Bisschop, S. E., Fraser, H. J., Öberg, K. I., van Dishoeck, E. F., & Schlemmer, S. 2006, A&A, 449, 1297

Caselli, P., Walmsley, C. M., Tafalla, M., Dore, L., & Myers, P. C. 1999, ApJ, 523, L165

Chiar, J. E., Adamson, A. J., Kerr, T. H., & Whittet, D. C. B. 1994, ApJ, 426, 240

Dartois, E., d'Hendecourt, L., Thi, W., Pontoppidan, K. M., & van Dishoeck, E. F. 2002, A&A, 394, 1057

Evans, N. J., Allen, L. E., Blake, G. A., et al. 2003, PASP, 115, 965

Gerakines, P. A., Schutte, W. A., Greenberg, J. M., & van Dishoeck, E. F. 1995, A&A, 296, 810

Jørgensen, J. K., Schöier, F. L., & van Dishoeck, E. F. 2005, A&A, 435, 177

Keane, J. V., Tielens, A. G. G. M., Boogert, A. C. A., Schutte, W. A., & Whittet, D. C. B. 2001, A&A, 376, 254

Lahuis, F., van Dishoeck, E. F., Boogert, A. C. A., et al. 2006, ApJ, 636, L145

Motte, F., Andre, P., & Neri, R. 1998, A&A, 336, 150

Pontoppidan, K. M., Dullemond, C. P., van Dishoeck, E. F., et al. 2005, ApJ, 622, 463

Pontoppidan, K. M., Fraser, H. J., Dartois, E., et al. 2003, A&A, 408, 981

Pontoppidan, K. M., van Dishoeck, E. F., & Dartois, E. 2004, A&A, 426, 925

Ridge, N. A., Di Francesco, J., Kirk, H., et al. 2006, AJ, in press

Schutte, W. A. & Khanna, R. K. 2003, A&A, 398, 1049

Tafalla, M., Myers, P. C., Caselli, P., & Walmsley, C. M. 2004, A&A, 416, 191

van Dishoeck, E. F., Dartois, E., Pontoppidan, K. M., et al. 2003, The Messenger, 113, 49

Whittet, D. C. B., Bode, M. F., Longmore, A. J., et al. 1988, MNRAS, 233, 321